ISSN 0023-1584, Kinetics and Catalysis, 2008, Vol. 49, No. 2, pp. 167–177. © MAIK "Nauka/Interperiodica" (Russia), 2008.
Original Russian Text © E.V. Gurentsov, A.V. Eremin, C. Schulz, 2008, published in Kinetika i Kataliz, 2008, Vol. 49, No. 2, pp. 179–189.

Effect of Active Impurities on the Condensation of Nanoparticles from Supersaturated Carbon Vapor in the Combined Laser Photolysis of C_3O_2 and H_2S

E. V. Gurentsov[a], A. V. Eremin[a], and C. Schulz[b]

[a] *Institute of Thermal Physics of Extreme States, Russian Academy of Sciences, Moscow, 125412 Russia*
[b] *Institut für Verbrennung und Gasdynamik, 47048 Duisburg, Germany*
e-mail: gurentsov@ihed.ras.ru

Received January 25, 2007

Abstract—The effect of active H_2S, $HS^{\bullet}$, and atomic hydrogen impurities on the condensation of highly supersaturated carbon vapor obtained in the combined laser photolysis of a mixture of C_3O_2 and H_2S diluted with argon was studied. The concentrations of carbon vapor, $HS^{\bullet}$, and atomic hydrogen obtained in the laser photolysis of the mixture were determined using the absorption cross sections of C_3O_2 and H_2S molecules measured in this work and the measured amount of absorbed laser radiation. The time profiles of the sizes of growing nanoparticles synthesized in C_3O_2 + Ar and C_3O_2 + H_2S + Ar mixtures were measured using the laser-induced incandescence (LII) method. An improved LII model was developed, which simultaneously took into account the heating and cooling of nanoparticles and the temperature dependence of the thermophysical properties of nanoparticles, as well as the cooling of nanoparticles by evaporation and thermal emission. The size distributions of carbon nanoparticles formed in the presence and absence of active impurities were determined with the use of a transmission electron microscope. The final average size of carbon nanoparticles was found to decrease from 12 to 9 nm upon the addition of H_2S to the system, whereas the rate of nanoparticle growth decreased by a factor of 3, and the properties of nanoparticles changed. In particular, the translational energy accommodation coefficient for Ar molecules at the surface of carbon nanoparticles was found to decrease from 0.44 to 0.30. A comparison of the calculated total carbon balance at the early stages of nanoparticle formation with experimental data demonstrated that the reaction $C + H_2S \longrightarrow HCS^{\bullet} + H$, which removes a portion of carbon vapor from the condensation process, has a determining effect on the carbon balance in the system. It was found that $HS^{\bullet}$ and atomic hydrogen affect the carbon balance in the system only slightly. Thus, the experimentally observed decrease in the rate of nanoparticle growth and in the sizes of nanoparticles can be explained by a decrease in the concentration of free carbon upon the addition of H_2S molecules to the system.

DOI: 10.1134/S002315840802002X

INTRODUCTION

The effects of various impurities on the kinetics of formation of carbon nanoparticles in combustion processes are of interest because of a wide variety of practically occurring conditions. In particular, in the kinetic simulation of the combustion of sulfur-containing coals and hydrocarbon fuels, the mechanisms of action of various active impurities (including sulfur-containing impurities) should be known in order to solve problems related to the promotion or inhibition of soot formation [1, 2]. Moreover, processes occurring in interstellar clouds, which are rich in atomic carbon and contain considerable sulfur-containing impurities, are of fundamental interest [3].

A few works on the experimental and theoretical studies of only the effect of hydrogen on the formation of carbon nanoparticles have been published. Starikovsky et al. [4] performed such a study in a shock tube for the CCl_4–H_2–Ar system. Dorge et al. [5] attempted to determine the effect of molecular hydrogen additives (0.33%) on the growth of carbon nanoparticles in the pyrolysis of a mixture of 0.33% C_3O_2 + Ar. Frenklach [6] theoretically considered the participation of atomic hydrogen, which resulted from the dissociation of complex hydrocarbon molecules, in the growth of soot particles. The variety of experimental conditions and proposed mechanisms does not allow one to make an unambiguous conclusion on the role of hydrogen additives in the formation of carbon nanoparticles. Schofield [1] considered in detail the kinetics of flame brining in the presence of sulfur-containing impurities; however, he did not analyze the processes of soot formation in the cited publication. According to Petzold et al. [2], the effect of sulfur-containing impurities on the formation of nanoparticles in the exhaust gases of internal-combustion engines is based on competition between carbon and sulfuric acid condensation processes. Therefore, an increase in the amount of sulfur-

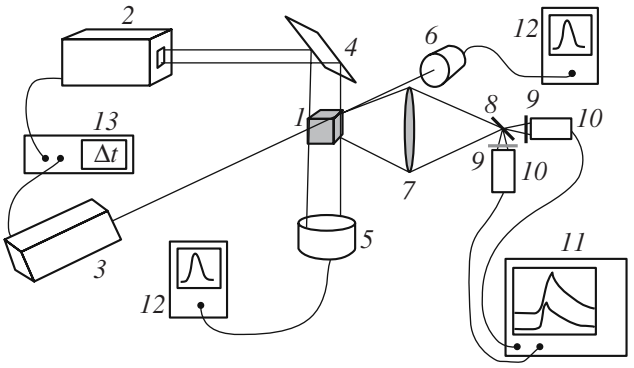

Fig. 1. Schematic diagram of the experimental setup: (*1*) photolytic cell, (*2*) excimer laser, (*3*) Nd:YAG laser, (*4*) dielectric mirror, (*5*, *6*) energy meters, (*7*) converging lens, (*8*) quartz plate, (*9*) optical narrow-band filters (550 and 694 nm), (*10*) photomultiplier tube, (*11*, *12*) oscilloscopes, and (*13*) delayed pulse oscillator.

containing substances in fuel results in the inhibition of the growth of carbon nanoparticles because of the active condensation of sulfuric acid on carbon clusters. Although Yamada et al. [3] discussed the reaction paths of atomic carbon with the sulfur-containing molecules H_2S, $HS^{\bullet}$, S, etc., in cosmic molecular clouds, the effect of sulfur-containing impurities on the formation of carbon nanoparticles in the condensation of carbon vapor has not been considered in the literature. Thus, note that the effect of active sulfur-containing impurities and atomic hydrogen on the formation of carbon nanoparticles is not clearly understood, whereas quantitative data are required for the kinetic simulation.

For an experimental study of the above problem, it seemed reasonable to compare the processes of nanoparticle condensation from pure carbon vapor and with the addition of active sulfur-containing compounds and atomic hydrogen. The carbon suboxide C_3O_2 mixed with a diluent gas is the most convenient precursor of pure carbon vapor [7]. The formation of carbon nanoparticles in this system was studied in shock tubes [8–10] and in a photolytic cell [11, 12].

In this study, we used a method for the generation of supersaturated carbon vapor under the UV photolysis of a mixture of C_3O_2 with argon at room temperature as described in previous publications [11, 12]. The conditions of UV photolysis are characterized by good predictability and the uniformity of parameters (concentration and pressure) in the instantaneously obtained carbon vapor in the test volume. Moreover, the time profiles of the size of growing carbon nanoparticles (these time profiles are of importance for the development of kinetic mechanisms of nanoparticle growth) can be studied using this method with minimum experimental work, as compared, for example, with the studies in shock tubes. It is also important that this method has no limitations on the process observation time.

In this study, we used the combined photolysis of a mixture of C_3O_2 and H_2S diluted with argon in order to introduce active impurities into the reacting system. In the absorption of UV photons with a wavelength of 193 nm, a portion of photons was absorbed by C_3O_2 molecules to yield a C atom and two CO molecules [13], whereas the other portion absorbed by H_2S molecules participated in the formation of atomic hydrogen and the $HS^{\bullet}$ radical [13].

Thus, the main goal of this study was to obtain quantitative kinetic data on the formation of carbon nanoparticles in the condensation of carbon vapor with H_2S, $HS^{\bullet}$, and atomic hydrogen impurities; to determine the properties of the resulting nanoparticles; and to compare them with the properties of nanoparticles formed from pure carbon vapor.

EXPERIMENTAL

Synthesis of Nanoparticles

Figure 1 shows a schematic diagram of the experimental setup. The synthesis of nanoparticles was performed at room temperature in a 0.5-cm^3 quartz cell, which was preevacuated and then filled with a prepared mixture of 10 mbar C_3O_2 + 1 bar Ar or 10 mbar C_3O_2 + 1 mbar H_2S + 1 bar Ar. A Lambda Physics EMG 150TMSC argon–fluorine excimer laser, which generated radiation at the wavelength λ = 193 nm with a pulse duration of 20 ns and a maximum pulse energy of 100 mJ, was used as a source of photons for the photodissociation of C_3O_2 and H_2S molecules. The laser beam with a rectangular cross section was focused using a cylindrical quartz lens so that its cross section coincided with the surface area of a cell face. In order to determine the total energy absorbed by C_3O_2 and H_2S molecules, the energy of radiation transmitted through the evacuated cell was measured using a calibrated calorimeter before each particular experiment and the energy of radiation transmitted through the cell filled with the prepared mixture was measured in the course of an experiment.

Previously, the absorption of laser radiation by either of the individual substances was measured at various concentrations and dilutions with argon. The absorption cross sections of C_3O_2 and H_2S molecules at λ = 193 nm were determined. They were found equal to 9×10^{-19} and 4.6×10^{-18} cm^2, respectively; these values are consistent with published data [13].

The concentrations of carbon and hydrogen atoms formed in the flash photolysis of a mixture of C_3O_2 and H_2S were determined from the measured total absorbed energy based on the assumption that one C atom and two CO molecules or one H atom and an $HS^{\bullet}$ radical are formed upon the absorption of a photon [13] with the use of the measured absorption cross sections. Table 1 summarizes the thus-determined concentrations of C, H, and $HS^{\bullet}$. Moreover, C_3O_2 (~9 mbar) and H_2S (~0.6 mbar) molecules undegraded as a result of

photodissociation were present in the system after a laser pulse. The effect of these molecules on the condensation of carbon nanoparticles was taken into consideration in the subsequent interpretation of the experimental data. In these experiments, the optically thin layer conditions of photoabsorption were retained; therefore, the concentration nonuniformity of C and H atoms along a laser beam was considered negligibly small. The concentration nonuniformity of C and H atoms due to the nonuniform spatial distribution of laser radiation energy was ignored in this work. By our estimates, the spatial nonuniformity of photodissociation product concentrations leveled by diffusion in the given volume in a few microseconds. The error in concentration measurements arose from an instrumental error of laser radiation energy measurements, an error in absorption cross section measurements, and an error due to the instability of laser radiation energy from pulse to pulse. The error in the determination of carbon vapor and atomic hydrogen concentrations was 20%.

The condensation of nanoparticles from supersaturated carbon vapor in the test volume occurred within 50–150 μs. In the condensation of carbon vapor into nanoparticles of size 10 nm, the heat release can be as high as 100 kJ/mol. By our estimates, the finite increase in the temperature of a mixture was no higher than 10–30 K under the experimental test conditions; therefore, the temperature effect of condensation was ignored in this work.

Table 1. Photolysis product concentrations (cm^{-3}) in a mixture of 10 mbar C_3O_2 + 1 mbar H_2S in argon

C	H	HS
$(2.72 \pm 0.5) \times 10^{16}$ (1.1 mbar)	$(1.08 \pm 0.2) \times 10^{16}$ (0.4 mbar)	$(1.08 \pm 0.2) \times 10^{16}$ (0.4 mbar)

Electron Microscopy

To obtain the electron micrographs of samples in the course of experiments, we deposited nanoparticles onto grids placed at the bottom of a quartz cell. Figures 2 and 3 show the micrographs of nanoparticles formed in the test mixtures and nanoparticle size distribution histograms, which were obtained from an analysis of the electron micrographs. The histograms were approximated by calculated curves constructed using a lognormal distribution function. The best fit to experimental

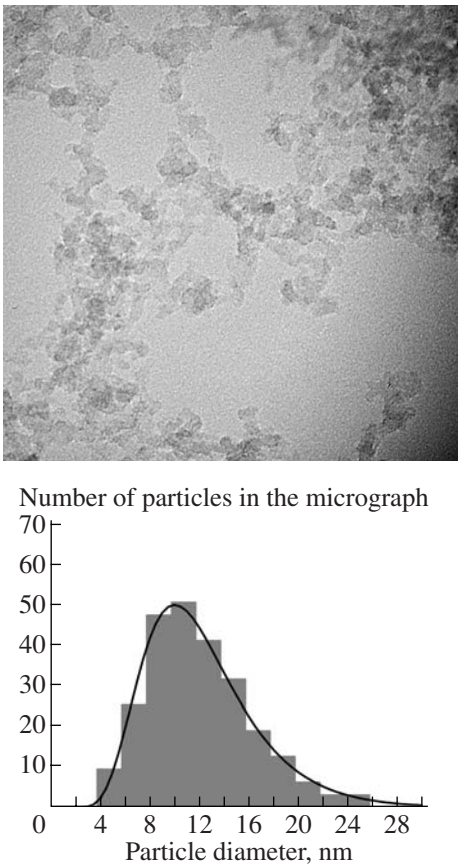

Fig. 2. Micrograph and size distribution of nanoparticles prepared by the photolysis of a mixture of 10 mbar C_3O_2 + 1 bar Ar.

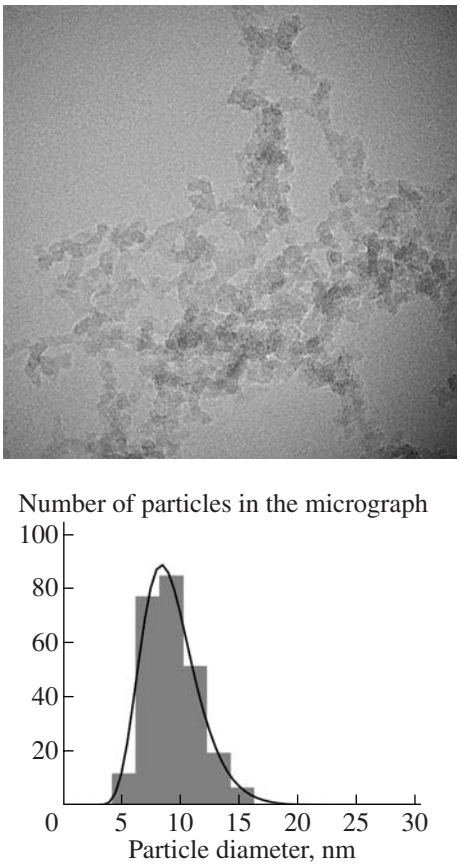

Fig. 3. Micrograph and size distribution of nanoparticles prepared by the photolysis of a mixture of 10 mbar C_3O_2 + 1 mbar H_2S + 1 bar Ar.

data for a mixture of C_3O_2 diluted with argon was obtained at the average nanoparticle size d_a = 11.5 nm and the geometric deviation from the average size σ_g = 1.3, whereas the values of d_a = 9 nm and σ_g = 1.2 were found for a mixture of C_3O_2 with an H_2S additive in argon.

Laser-Induced Incandescence Measurements of Current Nanoparticle Sizes

The previously developed method of laser-induced incandescence (LII) [14–18] was used for measuring the sizes of formed nanoparticles. The LII method is based on measuring emission from nanoparticles heated by a short laser pulse with a duration of a few microseconds. As a result of heating in a short time, the emission reached a maximum and then decayed because of nanoparticle cooling with the surrounding gas molecules. The time of cooling depended on the size and thermophysical properties of nanoparticles and on the surrounding gas characteristics.

In this study, a pulsed Nd:YAG laser (Quanta Ray DCR11), which generated radiation at λ = 1064 nm and a pulse halfwidth time of about 10 ns, was used as a radiation source for heating nanoparticles. The cross section of the laser beam that acted on particles was a disk 1 mm in diameter, which was obtained by diaphragming an initial beam 8 mm in diameter. The energy distribution over the cutout beam diameter was considered uniform. The energy density in a pulse lay in the range 0.2–0.7 J/cm^2. The time profiles of incandescence were measured using Hamamatsu R7400 U-4 photomultiplier tubes with signal amplifiers at two wavelengths with the use of optical narrow-band filters with transmission maximums at 550 and 694 nm. The LII signals were recorded with a LeCroy LT 342 digital oscilloscope with a frequency bandwidth of 500 MHz. The time resolution of the detection system was 2 ns or better. Figure 1 shows a schematic diagram of LII measurements.

LII MODEL

The theory of LII is based on mass and energy conservation laws (Eqs. (1) and (2), respectively) in the processes of heating and the subsequent cooling of a spherical particle with a laser beam [14–18]:

$$\frac{\mathrm{d}(m_p c_p T_p)}{\mathrm{d}t} = \dot{q}_{abs} - \dot{q}_{rad} - \dot{q}_{cond} - \dot{q}_{evap}; \quad (1)$$

$$\frac{\mathrm{d}m_p}{\mathrm{d}t} = -J_{evap}, \quad (2)$$

where m_p and c_p are the mass and heat capacity of nanoparticles, respectively; T_p is the current temperature of nanoparticles; t is time; J_{evap} is the mass flow from the surface of nanoparticles because of evaporation; $\dot{q}_{abs}$ is the laser energy flux absorbed by the surface of nanoparticles; and $\dot{q}_{evap}$, $\dot{q}_{rad}$, and $\dot{q}_{cond}$ are the energy fluxes from the surface of nanoparticles in the processes of evaporation, thermal radiation, and conductive heat exchange with surrounding gas molecules, respectively.

Laser Heating of Nanoparticles

In this model, the processes of heating and cooling overlapped in time; this allowed us to obtain results with a better accuracy than that reported in early publications [10, 12, 19–21], in which cooling was taken into consideration from the point in time at which the laser was switched off. For this purpose, a dimensionless model time-resolved laser-energy distribution function $j(t)$ was introduced into the calculation as a Gaussian distribution curve with a halfwidth of 10 ns. Using the measured integrated laser energy flux density R_0 (J/cm^2) normalized to the integral of the function $j(t)$ over a pulse time, we can write the energy flux absorbed by the surface of a spherical particle with the diameter d_p as [22]

$$\dot{q}_{abs} = \pi^2 d_p^3 \frac{F}{\lambda_{laser}} \frac{R_0 j(t)}{\int j(t')\mathrm{d}t'}, \quad (3)$$

where λ_{laser} is the heating laser wavelength and F is a function that depends on the optical properties of nanoparticles:

$$F = -\mathrm{Im}\left(\frac{m^2-1}{m^2+2}\right) = \frac{6nk}{(n^2-k^2+2)^2+4n^2k^2}; \quad (4)$$

here, $m = n - k\mathrm{i}$ is the complex refraction index.

In the Rayleigh approximation ($d_p \ll \lambda_{laser}$), the heating of a nanoparticle because of the absorption of laser radiation can be considered uniform over the volume as a consequence of the high thermal conductivity of the nanoparticle material [15]. In the calculation of energy absorbed by a nanoparticle, the greatest uncertainty consists in the determination of the value of F, which depends on the wavelength of incident radiation and the surface structure of the nanoparticle. In accordance with published data [23], the value of m = 1.57 – 0.56i (F = 0.26), which has been most frequently recommended in the literature for soot nanoparticles, was used in this work. Note that, in the case of the formation of carbon nanoparticles from pure carbon vapor, the value of F can differ from the recommended value [23]. Petzold et al. [2] proposed the use of the refraction index m = 1.57 – 1.4i, which corresponds to F = 0.51, in order to explain experimental data of the integral yield of soot in the pyrolysis of C_3O_2 in argon. However, varying the value of F over the range 0.26–0.51 in this model resulted in a change in nanoparticle sizes by no more than 15% at a laser radiation wavelength of 1064 nm. This occurred because the value of F most strongly affected the maximum temperature of heating and only slightly affected the time of nanoparticle cool-

ing, which is directly related to the size of nanoparticles. The maximum temperature of nanoparticle heating (T_p^0) is determined from the equation

$$T_p^0 = T_g + \frac{6\pi R_0 F}{\rho_p c_p \lambda_{laser}}, \quad (5)$$

where ρ_p is the density of nanoparticles.

Moreover, two-color pyrometry, which was described by Kock et al. [24], can be applied to measure the maximum temperature of nanoparticle heating using the LII signals detected at two wavelengths. The maximum temperatures of nanoparticle heating found in this work by two-color pyrometry on the one hand and from Eq. (5) with the use of the measured laser energy and the refraction index $m = 1.57 - 0.56i$ on the other hand differed by no more than 10%.

Nanoparticle Cooling in the Course of Conductive Heat Exchange

The conditions of heat exchange between nanoparticles and a surrounding gas are determined by the Knudsen number (the ratio of the mean free path length of the gas molecules to the characteristic length of a particle). In this study, the Knudsen number was much greater than 1 ($Kn \gg 1$) in all of the experimental regimes; this corresponds to a free molecular heat exchange regime. As can be seen in Figs. 2 and 3, the primary nanoparticles were combined into aggregates rather than isolated from each other. The effect of nanoparticle aggregation was relatively small in the case of the free molecular heat exchange regime between the particle and the surrounding gas because the efficiency of heat exchange depends on the nanoparticle surface area. In this approach, the decrease in the apparent surface area of nanoparticles upon their aggregation was considered insignificant. According to Williams and Loyalka [25], the energy flux from the particle to the surrounding gas because of free molecular heat exchange can be written as follows:

$$\dot{q}_{cond} = \alpha\pi d_p^2 \frac{P}{2}\sqrt{\frac{8k_B T_g}{\pi\mu_g}}\left(\frac{\gamma+1}{\gamma-1}\right)\left(\frac{T_p(t)}{T_g} - 1\right), \quad (6)$$

where T_g is the temperature of the surrounding gas atmosphere, k_B is the Boltzmann constant, α is the translational energy accommodation coefficient for the collision of a diluent gas molecule with the particle surface, μ_g is the molar mass of the diluent gas, P is the total pressure of the mixture, and γ is the adiabatic index of the diluent gas. The temperature of the gas atmosphere was considered constant because the laser-heated volume was small (3% of the entire cell volume).

The accommodation coefficient, which is chosen based on known data or is a model parameter, has the greatest uncertainty in the above expression. The value of α depends on the structure and material of nanoparticles, the temperature of the atmosphere, and the type of the diluent gas. Based on various sources, the accommodation coefficients for soot particles fall in the range of 0.26 to 0.90 [26]. In this work, we a priori used the accommodation coefficient $\alpha = 0.44$, which was experimentally obtained in similar experiments [12] for carbon nanoparticles in argon.

Nanoparticle Cooling on Evaporation

The process parameters of nanoparticle evaporation because of laser heating to temperatures higher than the evaporation temperature of carbon (about 4000 K) were determined using published relationships [27]. The heat flux removed from the surface of a nanoparticle because of evaporation can be written as

$$\dot{q}_{evap} = J_{evap}\Delta H_v, \quad (7)$$

where ΔH_v is the heat of vaporization and J_{evap} is the amount of substance removed from the nanoparticle surface:

$$J_{evap} = \frac{1}{\mu}\frac{dM}{dt}. \quad (8)$$

Here, μ is the molar mass of evaporating molecules. The mass change of a spherical nanoparticle depends on the molecular flow from the surface:

$$\frac{dM}{dt} = -\frac{\pi}{4} d_p^2 \rho_v \upsilon_v, \quad (9)$$

where ρ_v and υ_v are the density and average thermal velocity of saturated vapor molecules over the surface of a spherical nanoparticle, respectively. The average thermal velocity of evaporating molecules was determined as

$$\upsilon_v = \sqrt{\frac{8RT_p}{\pi\mu}}. \quad (10)$$

According to Smallwood et al. [27], the statement that C_3 clusters with the molar mass $\mu = 36$ g/mol escaping from the surface of a spherical particle make the main contribution to evaporation was used in this work.

The value of ρ_v was calculated using the ideal gas state equation

$$\rho_v = \frac{P_v \mu}{RT_p}. \quad (11)$$

The saturated vapor pressure P_v over the surface of a spherical particle was determined from the Clapeyron–Clausius equation

$$P_v = p^* \exp\left(-\frac{\Delta H_v}{R}\left(\frac{1}{T_p} - \frac{1}{T^*}\right)\right), \quad (12)$$

where $p^* = 0.0006071$ atm and $T^* = 3000$ K are the pressure and temperature of carbon, respectively, at a critical point [28]; $\Delta H_v = 834010.56$ J/mol is the heat of evaporation of carbon; R is the gas constant; and T_p is the nanoparticle surface temperature.

Nanoparticle Cooling by Emission

The radiation heat flow at maximum temperatures of carbon nanoparticles (higher than 4000–5000 K) heated by laser radiation can be comparable in magnitude with the conductive heat flow in a short time. Therefore, radiation heat losses should be considered in order to construct the calculated LII signal profile as a function of time. However, note that the effect of the radiation flow on the determined nanoparticle size was found insignificant (to within 1%) at the temperatures of nanoparticle heating in these experiments to 3500 K. The thermal radiation flux from a heated spherical nanoparticle was determined from Planck's law for a blackbody according to Michelsen [22]:

$$\dot{q}_{\text{rad}} = \pi d_{\text{p}}^2 \int_0^\infty \varepsilon_\lambda \frac{2\pi hc^2}{\lambda^5 [\exp(hc/\lambda k_{\text{B}} T_{\text{p}}) - 1]} \text{d}\lambda, \quad (13)$$

where $\varepsilon_\lambda = 4\pi d_{\text{p}} F/\lambda$ is the radiating capacity of a nanoparticle, h is the Planck constant, and c is the speed of light in a vacuum. Taking into account that the effect of radiation cooling was small, as a first approximation, we used the quantity F, which is independent of wavelength; this is true for soot nanoparticles in the visible and IR regions [22].

Additional Refinements of the Model

In this work, the heat capacity of the nanoparticle material was taken equal to the heat capacity of solid graphite, as was done by Starke et al. [19]. Because the heat capacity considerably changed upon laser heating from room temperature to 3000–4000 K, polynomial approximations were used in the model for the temperature dependence of the heat capacity of graphite [29]:

$$C_{\text{p}} = a + bT + cT^2 \ [\text{J K}^{-1} \text{ mol}^{-1}], \quad (14)$$

where $a = 16.86$ J K^{-1} mol^{-1}, $b = 0.00477$ J K^{-2} mol^{-1}, and $c = 854000$ J K^3 mol^{-1}.

Lehre et al. [30] found that the use of a monodisperse approximation for the nanoparticle size distribution can result in considerable determination errors in the average diameter of nanoparticles. In this work, we used a lognormal nanoparticle size distribution, which is most commonly encountered in nature [31]. The expression for the probability density of the lognormal nanoparticle size distribution (df) is written as

$$\text{d}f = \frac{1}{\sqrt{2\pi} d_{\text{p}} \ln\sigma_{\text{g}}} \exp\left[\frac{(\ln d_{\text{p}} - \ln d_{\text{a}})^2}{2(\ln\sigma_{\text{g}})^2}\right] \text{d}d_{\text{p}}, \quad (15)$$

where d_{a} is the average nanoparticle size in the lognormal distribution and σ_{g} is the geometric deviation from the average size.

To interpret the experimental LII signals, the value of σ_{g} was determined from an analysis of the electron micrographs of nanoparticle samples (Figs. 2, 3) taken in the course of experiments.

Emission Signal Calculation

The emission intensity $J(t)$ of laser-heated nanoparticles at a specified wavelength with consideration for the contribution of a nanoparticle size distribution was determined as

$$J(t) = \int_{d_{\text{p1}}}^{d_{\text{p2}}} S(t) \text{d}f. \quad (16)$$

The emission signal at the detected wavelength to within a constant C was determined from the following equations, which were derived by Roth and Filippov [15] assuming the Planck emission spectrum of heated nanoparticles:

$$S(t) = C\left[\frac{1}{\exp\left(\frac{hc}{\lambda k_{\text{B}} T_{\text{p}}(t)}\right) - 1} - \frac{1}{\exp\left(\frac{hc}{\lambda k_{\text{B}} T_{\text{g}}}\right) - 1}\right], \quad (17)$$

where λ is the wavelength chosen for the detection of LII radiation.

The time dependence of the nanoparticle temperature T_{p} was determined by solving a set of differential Eqs. (1) and (2) using the second order Runge–Kutta method. The experimentally obtained oscillograms of LII radiation in the region of cooling were approximated with calculated curves by varying the average size. Figure 4 shows an LII signal detected experimentally and its approximation by calculated curves.

As a result of LII measurements, the average sizes of nanoparticles were determined at various times from the instant of carbon vapor formation (over a range from 5 to 10^5 μs); thus, the time profiles of the sizes of growing particles in the test mixtures were obtained.

RESULTS

To determine the size of nanoparticles by the LII method in this work, we used an accommodation coefficient of 0.44, which was found previously [12] for carbon nanoparticles obtained in the photolysis of C_3O_2 in a mixture with argon. As in the previous study [12], the use of the specified value resulted in a good correspondence between the ultimate sizes of nanoparticles, which were synthesized in the above mixture, measured using the LII method and electron microscopy. However, for carbon nanoparticles synthesized in a mixture of C_3O_2 with an additive of H_2S, the sizes found by the LII method on the assumption that $\alpha = 0.44$ were 30% greater than those measured using electron microscopy. By comparing the sizes of nanoparticles obtained by two different methods and assuming that the density and heat capacity of nanoparticles changed only slightly upon the addition of active impurities as compared to pure carbon nanoparticles, the accommodation coefficient $\alpha = 0.30$ was determined for the nanoparticles synthesized in a mixture of C_3O_2

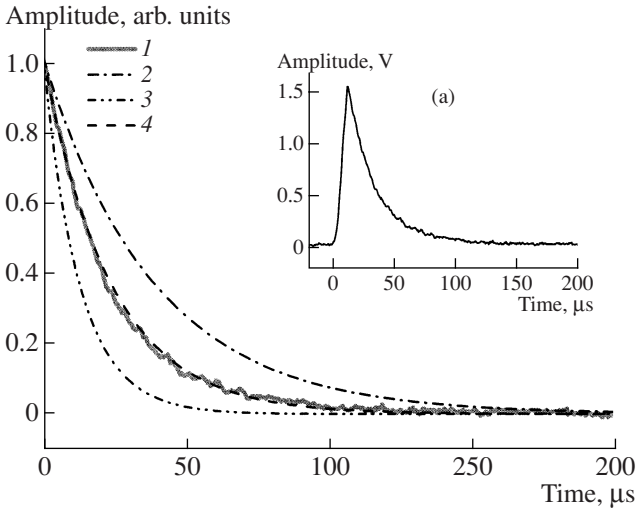

Fig. 4. (a) LII signal and the approximation of a cooling portion of the LII signal by calculated curves at various average nanoparticle diameters: (*1*) an experimental signal and (*2–4*) calculations for d_a = (*2*) 16, (*3*) 8, and (*4*) 12 nm.

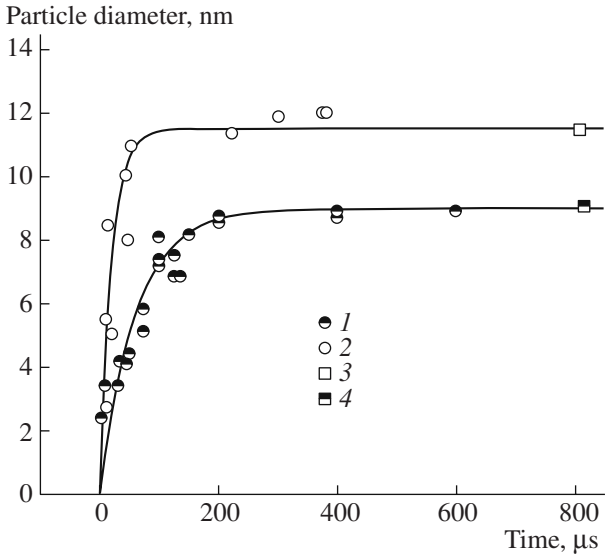

Fig. 5. Time profiles of the sizes of nanoparticles obtained by the photolysis of the mixtures of (*1*) 10 mbar C_3O_2 + 1 mbar H_2S + 1 bar Ar and (*2*) 10 mbar C_3O_2 + 1 bar Ar and (*3*, *4*) corresponding electron-microscopic data. Points and curves refer to experimental data and approximation by empirical functions derived by Butland and Maddison [29].

with H_2S. This value is close to $\alpha = 0.23–0.38$, which was recommended by Snelling et al. [26] for soot nanoparticles.

Figure 5 shows the time profiles of the sizes of nanoparticles synthesized in pure C_3O_2 + Ar and C_3O_2 + H_2S + Ar obtained using the LII method and electron-microscopic data on the final nanoparticle sizes. The experimental data in Fig. 5 are generalized using empirical functions for the profiles of carbon nanoparticle sizes obtained in our previous study [32]. In Fig. 5, it can be seen that the time of growth to the final sizes of nanoparticles formed in the mixture with no H_2S additive was much shorter (~50 μs) than that for nanoparticles whose condensation occurred in the presence of H_2S, $HS^{\bullet}$, and atomic hydrogen impurities (~150 μs). In other words, the rate of growth of nanoparticles in the absence of the above active additives was higher. Moreover, the average size of final nanoparticles synthesized from pure carbon vapor was 12 nm, whereas the average size of nanoparticles formed in a mixture with added H_2S was smaller and equal to 9 nm.

DISCUSSION

To study the effect of active impurities on the formation of carbon nanoparticles and to interpret the resulting experimental data, we considered a kinetic scheme of the consumption of carbon atoms at the early stages of the process of carbon vapor condensation (Table 2). The kinetic scheme includes the consumption reactions of carbon atoms formed by the photodissociation of C_3O_2; reactions with the participation of H, H_2, and $SH^{\bullet}$; and hydrocarbon formation reactions. Note that the considered process conditions at room temperature were dramatically different from combustion conditions in flames and internal combustion engines, under which most kinetic data were obtained. This circumstance was responsible for the choice of reactions and constants characteristic of room temperatures. The CHEMKIN II program package was used for calculations in accordance with the given kinetic mechanism. The initial concentrations of starting substances, the pressure, and the temperature were chosen in accordance with the experimental conditions.

The main consumption of C atoms in the absence of other impurities was due to reaction (II), which is the initial step of carbon vapor condensation. It is most likely that reaction (II) is a three-particle reaction, although it was considered previously as a two-particle reaction [8, 33]. This approach results from the fact that the reaction is of second order in the limit of high pressures. Previously [32], we found that the limit of high pressures in the addition of the carbon atom to a carbon cluster occurred at 200–300 mbar under the conditions of the given experiments. In the kinetic scheme, the rate constant of reaction (II) from [33] was used as the best suited for temperature conditions. However, note that the problem of the reaction rates of formation and decay of C_2, C_3, …, C_n clusters remains inadequately solved [8]. The further growth of carbon nanoparticles was due to the formation of condensation centers (clusters containing 6–30 atoms) and the addition of carbon atoms and smaller carbon clusters to these centers [3, 8, 32]. Under the conditions of this experiment, it is important to consider reaction (III), which can result in a considerable consumption of C atoms and the synthesis of C_2 due to C_3O_2 molecules undegraded in photodissociation. The rate constant of reaction (III) was

Table 2. Kinetic reaction scheme of the consumption of carbon vapor at the early stages of nanoparticle formation in the system with active additives

Reaction	$k = A(T)^b \exp(-E_a/RT)$, $cm^3\ mol^{-1}\ s^{-1}$			Reference
	A	b	E_a, kJ/mol	
Consumption of carbon atoms				
$C + H_2S \longrightarrow HCS^{\bullet} + H$ (I)	1.27×10^{14}	0.0	0.0	[37]
$C + C \longrightarrow C_2^{\bullet\bullet}$ (II)	1.30×10^{13}	0.0	0.0	[33]
$C + C_3O_2 \longrightarrow 2CO + C_2^{\bullet\bullet}$ (III)	1.12×10^{15}	–1.75	0.0	[34]
″	3.60×10^{14}	0.0	23	[7]
″	1.08×10^{14}	0.0	0.0	[35]
$C + H_2 \longrightarrow CH_2^{\bullet\bullet}$ (IV)	1.03×10^{13}	0.0	0.0	[34]
Consumption of H atoms and formation of H_2				
$H + H + M \longrightarrow H_2 + M$ (V)	3.08×10^{15}	0.0	0.0	[38]
$H + H_2S \longrightarrow H_2 + SH^{\bullet}$ (VI)	5.18×10^{11}	0.0	0.0	[39]
$H + SH^{\bullet} \longrightarrow H_2 + S$ (VII)	1.30×10^{13}	0.0	0.0	[40]
$CO + H + M \longrightarrow HCO^{\bullet} + M$ (VIII)	5.79×10^{13}	0.0	0.0	[41]
$H + CH^{\bullet} \longrightarrow H_2 + C$ (IX)	8.43×10^{12}	0.0	0.0	[42]
$HCO^{\bullet} + HCO^{\bullet} \longrightarrow CO + CO + H_2$ (X)	2.19×10^{13}	0.0	0.0	[43]
$H + C_3O_2 \longrightarrow CO + HCCO^{\bullet}$ (XI)	1.18×10^{11}	0.0	0.0	[44]
Secondary reactions with S				
$S + SH^{\bullet} \longrightarrow S_2 + H$ (XII)	2.74×10^{13}	0.0	0.0	[40]
$SH^{\bullet} + SH^{\bullet} \longrightarrow S + H_2S$ (XIII)	2.40×10^{13}	0.0	0.0	[45]
Formation of hydrocarbons				
$CH^{\bullet} + CH^{\bullet} \longrightarrow C_2H_2$ (XIV)	1.20×10^{14}	0.0	0.0	[46]
$CH^{\bullet} + H_2 \longrightarrow CH_3^{\bullet}$ (XV)	1.21×10^{14}	0.0	0.0	[47]
$CO + CH^{\bullet} \longrightarrow HCCO^{\bullet}$ (XVI)	4.16×10^{12}	0.0	0.0	[48]
$CH_2^{\bullet\bullet} + H_2 \longrightarrow CH_3^{\bullet} + H$ (XVII)	4.16×10^{9}	0.0	0.0	[49]
$CH_2^{\bullet\bullet} + H \longrightarrow CH^{\bullet} + H_2$ (XVIII)	3.00×10^{14}	0.0	0.0	[50]

studied at 1500–2000 K in shock tubes [7, 34]. Data obtained in the cited publications were consistent with each other. In this case, it was found that this reaction has an energy barrier at elevated temperatures; therefore, reaction (III) will not have an effect on the process of C_2 formation upon the extrapolation of the above constants to room temperature. At the same time, Haider and Husain [35] reported the rate constant of reaction (III) for room temperature. This constant is high so that the yield of C_2 molecules in the reaction volume (where C atoms and CO and C_3O_2 molecules were initially present) is limited by only the amount of C atoms in the system and is independent of the occurrence of other reactions given in Table 2. In other words, if the rate constant of reaction (III) taken from [35] is valid for the given experimental conditions, the additive of H_2S and its photolysis products have no effect on the condensation of carbon vapor. However, this is inconsistent with the experimental data shown in Fig. 5, which indicates that the addition of H_2S, H, and $HS^{\bullet}$ to the $C–C_3O_2$ system changed the rate of growth and the size of nanoparticles. Thus, the rate constant of reaction (III) obtained by Friedrichs and Wagner [7] was used in the subsequent kinetic analysis.

Figure 6 shows the calculated time profiles of the concentrations of carbon atoms and C_2 molecules in the system where carbon vapor and CO and C_3O_2 molecules initially occurred in the absence of H, $HS^{\bullet}$, and H_2S; this corresponds to conditions at the early stage of formation of pure carbon nanoparticles. In Fig. 6, it can be seen that, in the absence of the effects of other substances, the concentration of C atoms decreased by a factor of 2.5 in 1.5–2 μs in the course of formation of C_2 molecules; in this case, it is believed that all of the carbon participated in the subsequent formation of nanoparticles.

In a mixture of $C_3O_2 + H_2S + Ar$ after the pulsed action of UV radiation, in accordance with experimental conditions, considerable amounts of H, $HS^{\bullet}$, and H_2S were initially present in the system along with car-

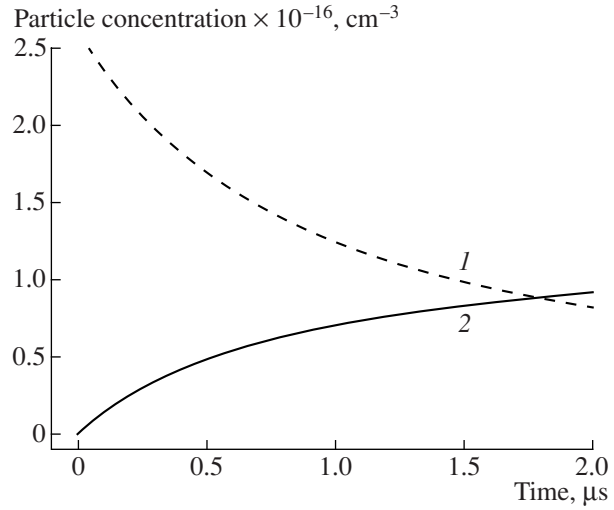

Fig. 6. Calculated dependence of the concentrations of (*1*) C and (*2*) C_2 on reaction time in a mixture of 1.1 mbar C + 8.9 mbar C_3O_2 + 1 bar Ar at 300 K.

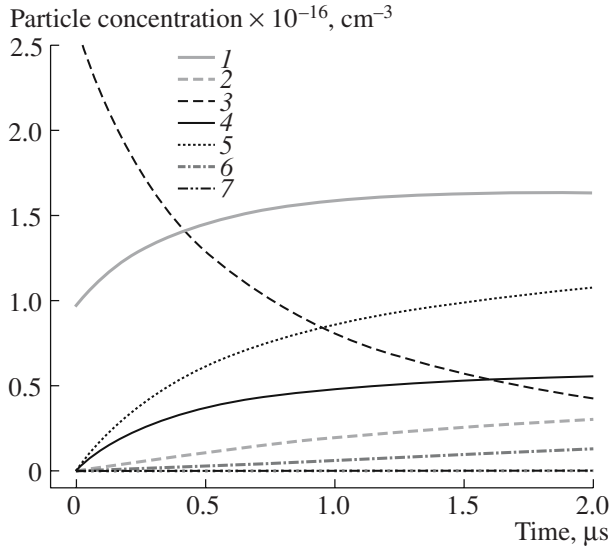

Fig. 7. Calculated dependence of the concentrations of various substances on reaction time in a mixture of 1.1 mbar C + 0.4 mbar H + 0.4 mbar HS + 0.6 mbar H_2S + 8.9 mbar C_3O_2 + 2.2 mbar CO + 1 bar Ar at 300 K: (*1*) H, (*2*) H_2, (*3*) C, (*4*) C_2, (*5*) $HCS^{\bullet}$, (*6*) $HCCO^{\bullet}$, and (*7*) $HCO^{\bullet}$.

bon vapor. Let us consider the effect of reactions with the participation of these substances on the balance of carbon in the system. Reactions (I) and (IV) were the main paths of carbon consumption. Reaction (I) resulted in the consumption of the initial amount of carbon vapor with the formation of $HCS^{\bullet}$ [36] in the interaction of atomic carbon with H_2S molecules undegraded as a result of pulse photodissociation. In this case, we failed to find any reaction paths of $HCS^{\bullet}$ consumption in interactions with the test substances in the literature. Therefore, we believe that reaction (I) mainly removed carbon from the nanoparticle condensation process. Reaction (IV) led to the consumption of atomic carbon with the formation of $CH_2^{\bullet}$. Molecular hydrogen was formed in reactions (V)–(VII), (IX), and (X). Note that there are no published data on the occurrence of the C + H forward reaction. Reactions (VIII) and (XI) can play a noticeable role in the balance of carbon in the system because of a considerable residual concentration of CO and C_3O_2 after the photodissociation of the mixture. Reactions (VIII) and (XI) led to the formation of $HCO^{\bullet}$ and $HCCO^{\bullet}$; in this case, carbon in these substances resulted from CO and C_3O_2 rather than carbon vapor.

Figure 7 shows the calculated concentration profiles of substances formed at the early stages of nanoparticle formation on the addition of H atoms, as well as $HS^{\bullet}$ and H_2S, in amounts corresponding to the experimental conditions to the reaction volume containing C atoms and CO and C_3O_2 molecules. The results of these calculations indicate that the concentration of atomic hydrogen increased with reference to its initial value in spite of the appearance of molecular hydrogen. In this case, any detectable consumption of carbon and formation of hydrocarbon molecules and radicals in reactions with hydrogen were not observed. The $HS^{\bullet}$ radical also had no detectable effect on the above concentration profiles of carbon-containing substances. In addition, note that the yield of C_2 decreased by a factor of 2, as compared with data given in Fig. 6; this resulted from the consumption of carbon atoms and the formation of $HCS^{\bullet}$ in reaction (I), which competes with the reaction path of C_2 formation. Thus, the formation of $HCS^{\bullet}$ in reaction (I) led to the considerable removal of the initial amount of carbon atoms from the nanoparticle condensation process, and, along with reaction (II), it was responsible for the balance of carbon in the system. An additional amount of carbon, which can participate in the formation of nanoparticles, appeared with the formation of $HCCO^{\bullet}$ in reaction (XI). Finally, in the calculations illustrated in Fig. 7, the total concentration of carbon atoms that occurred in an atomic state and as $C_2^{\bullet}$ radicals 2 μs after the appearance of carbon vapor was half as great as an analogous value for the conditions of calculations presented in Fig. 6. In this case, an analysis of concentrations sown in Fig. 7 demonstrated that the total amount of carbon as atoms, C_2, and other carbon-containing substances increased by only 8% because of the supply of carbon to the system from C_3O_2 by reaction (XI). Thus, the experimentally observed decrease in the rate of growth of carbon nanoparticles in the system with an H_2S additive (see Fig. 5) can be due to a twofold decrease in the initial concentration of carbon atoms at the early stages of nanoparticle formation because of the generation of the $HCS^{\bullet}$ radical. Previously [32], we reported data on the rates of growth of carbon nanoparticles from carbon vapor; these data are consistent with

the rate of nanoparticle growth observed in these experiments with the addition of H_2S. However, the concentration of carbon vapor in the previous study [32] was half as great.

Moreover, the difference between the volumes of final nanoparticles obtained from pure carbon vapor and from carbon vapor with an H_2S additive suggests that the amount of condensed carbon in the particles decreased by a factor of 2.

An experimentally observed change in the surface properties of nanoparticles, in particular, the above change in the accommodation coefficient upon the addition of H, $HS^{\bullet}$, and H_2S to the carbon vapor system, can be explained by the participation of a small amount of $HCS^{\bullet}$ or $HCCO^{\bullet}$ in the formation of the surface structure of carbon nanoparticles at the final stages of their growth.

CONCLUSIONS

The effect of H_2S, $HS^{\bullet}$, and atomic hydrogen additives on the formation of carbon nanoparticles from supersaturated carbon vapor at room temperature and atmospheric pressure in an atmosphere of argon was studied experimentally. An improved LII model was developed. This model simultaneously takes into account the heating and cooling of nanoparticles, the temperature dependence of the thermophysical properties of nanoparticles, and the cooling of nanoparticles by evaporation and radiation.

The sizes of nanoparticles synthesized from carbon vapor and in the system additionally containing H_2S, $HS^{\bullet}$, and atomic hydrogen were determined using LII and electron microscopy. It was found that the final average size of carbon nanoparticles decreased from 12 to 9 nm after the addition of the impurities. The time profiles of the sizes of growing carbon nanoparticles were obtained in both the presence of H_2S, $HS^{\bullet}$, and atomic hydrogen in the starting mixture and in the absence of these impurities. The time of nanoparticle growth to the final size was found to increase by a factor of 3 (from 50 to 150 μs) in the system with the active additives.

The translational energy accommodation coefficient of argon molecules at the surface of nanoparticles formed in the photolysis of a mixture of $C_3O_2 + H_2S +$ Ar was found. It was equal to 0.30, as opposed to a value of 0.44 found previously for the nanoparticles synthesized in the photolysis of a mixture of $C_3O_2 +$ Ar. The change in the accommodation coefficient is indicative of a change in the surface properties of nanoparticles because of the effect of an amount of $HCS^{\bullet}$ or $HCCO^{\bullet}$ on the condensation of carbon vapor.

The kinetic analysis of the balance of carbon at the early stages of carbon vapor condensation with the active additives demonstrated that a portion of carbon was removed from the condensation process because of the interaction with H_2S and the formation of $HCS^{\bullet}$ radicals. At the same time, small amounts of $HS^{\bullet}$ and atomic hydrogen did not have a considerable effect on the condensation of carbon vapor. The presence of H_2S in the system resulted in an inhibition of the formation of carbon nanoparticles and an increase in the nanoparticle size because of the conversion of about a half of the initial concentration of carbon vapor into $HCS^{\bullet}$ radicals, which mainly did not participate in the formation of carbon nanoparticles but did affect their properties.

ACKNOWLEDGMENTS

We are grateful to N. Schlosser (University of Duisburg) for performing electron microscopy analyses. This work was supported by the Russian Foundation for Basic Research and the German Research Foundation (DFG).

REFERENCES

1. Schofield, K., *Combust. Flame*, 2001, vol. 124, p. 137.
2. Petzold, A., Gysel, M., Vancassel, X., Hitzenberger, R., Puxbaum, H., Vrochticky, S., Weingartner, E., Baltensperger, U., and Mirabel, P., *Atmos. Chem. Phys.*, 2005, vol. 5, p. 3187.
3. Yamada, M., Osamura, Y., and Kaiser, R.I., *Astron. Astrophys.*, 2002, vol. 395, p. 1031.
4. Starikovsky, A., Thienel, Th., Wagner, H.Gg., and Zaslonko, I., *Ber. Bunsen-Ges. Phys. Chem.*, 1998, vol. 102, p. 1815.
5. Dorge, K.J., Tanke, D., and Wagner, H.Gg., *Z. Phys. Chem.*, 1999, vol. 212, p. 219.
6. Frenklach, M., *Proc. Combust. Inst.*, 1996, vol. 26, p. 2285.
7. Friedrichs, G. and Wagner, H.Gg., *Z. Phys. Chem.*, 1998, vol. 203, p. 1.
8. Vagner, Kh.G., Vlasov, P.A., Derge, K.Yu., Eremin, A.V., Zaslonko, I.S., and Tanke, D., *Kinet. Katal.*, 2001, vol. 42, no. 5, p. 645 [*Kinet. Catal.* (Engl. Transl.), vol. 42, no. 5, p. 583].
9. Vagner, Kh.G., Emel'yanov, A.V., Eremin, A.V., and Yander, Kh., *Kinet. Katal.*, 2003, vol. 44, no. 4, p. 509 [*Kinet. Catal.* (Engl. Transl.), vol. 44, no. 4, p. 463].
10. Starke, R., Kock, B., Roth, P., Eremin, A., Gurentsov, E., Shumova, V., and Ziborov, V., *Combust. Flame*, 2003, vol. 132, p. 77.
11. Emelianov, A., Eremin, A., Jander, H., and Wagner, H.Gg., *Z. Phys. Chem.*, 2003, vol. 217, p. 1361.
12. Eremin, A.V., Gurentsov, E.V., Hofmann, M., Kock, B., and Schulz, Ch., *Appl. Phys. B*, 2006, vol. 83, p. 449.
13. Okabe, H., *Photochemistry of Small Molecules*, New York: Wiley, 1978, p. 319.
14. Melton, L.A., *Appl. Opt.*, 1984, vol. 23, p. 2201.
15. Roth, P. and Filippov, A.V., *J. Aerosol Sci.*, 1996, vol. 27, p. 95.
16. Filippov, A.V., Marcus, M.W., and Roth, P., *J. Aerosol Sci.*, 1999, vol. 30, p. 71.
17. Mewes, B. and Seitzman, J.M., *Appl. Opt.*, 1997, vol. 36, p. 709.

18. Filippov, A.V. and Rosner, D.E., *Int. J. Heat Mass Transfer*, 2000, vol. 43, p. 127.
19. Starke, R., Kock, B., and Roth, P., *Shock Waves*, 2003, vol. 12, p. 351.
20. Gurentsov, E.V., Eremin, A.V., Shtarke, R., and Rott, P., *Kinet. Katal.*, 2005, vol. 46, no. 3, p. 333 [*Kinet. Catal.* (Engl. Transl.), vol. 46, no. 3, p. 309].
21. Eremin, A., Kokk, B., Rott, P., Shtarke, R., and Shumova, V., *Khim. Fiz.*, 2004, vol. 23, no. 9, p. 72.
22. Michelsen, H.A., *J. Chem. Phys.*, 2003, vol. 118, p. 7012.
23. Smyth, K.C. and Shaddix, C.R., *Combust. Flame*, 1996, vol. 107, p. 314.
24. Kock, B.F., Kayan, C., Knipping, J., Orthner, H.R., and Roth, P., *Proc. Combust. Inst.*, 2004, vol. 30, p. 1689.
25. Williams, M.R. and Loyalka, S.K., *Aerosol Science: Theory and Practice*, Oxford: Pergamon, 1991, p. 309.
26. Snelling, D.R., Liu, F., Smallwood, G.J., and Gulder, O.L., *Combust. Flame*, 2004, vol. 136, p. 180.
27. Smallwood, G.J., Snelling, D.R., Liu, F., and Gulder, O.L., *Trans. Am. Soc. Mech. Eng., J. Heat Transfer*, 2001, vol. 123, p. 814.
28. Leider, H.R., Krikorian, O.H., and Young, D.A., *Carbon*, 1973, vol. 11, p. 555.
29. Butland, A.T.D. and Maddison, R.J., *J. Nucl. Mater.*, 1973, vol. 49, p. 45.
30. Lehre, T., Jungfleisch, B., Suntz, R., and Bockhorn, H., *Appl. Opt.*, 2003, vol. 42, p. 2021.
31. Karasev, B.V., *Priroda*, 1995, no. 11, p. 41.
32. Gurentsov, E.V., Eremin, A.V., and Shul'ts, K., *Kinet. Katal.*, 2007, vol. 48, no. 2, p. 210 [*Kinet. Catal.* (Engl. Transl.), vol. 48, no. 2, p. 194].
33. Martinotti, F.F., Welch, M.J., and Wolf, A.P., *Chem. Commun.*, 1968, vol. 3, p. 115.
34. Dean, A.J., Davidson, D.F., and Hanson, R.K., *J. Phys. Chem.*, 1991, vol. 95, p. 183.
35. Haider, N. and Husain, D., *J. Chem. Soc., Faraday Trans.*, 1993, vol. 89, p. 7.
36. Kaiser, R.I., Sun, W., and Suits, A.G., *J. Chem. Phys.*, 1997, vol. 106, p. 5288.
37. Galland, N., Caralp, F., and Rayez, M.-T., Hannachi, Y., Loison, J.-C., Dorthe, G., and Bergeat, A., *J. Phys. Chem. A*, 2001, vol. 105, p. 9893.
38. Lynch, K.P., Schwab, T.C., and Michael, J.V., *Int. J. Chem. Kinet.*, 1976, vol. 8, p. 651.
39. Husain, D. and Slater, N.K.H., *J. Chem. Soc., Faraday Trans.*, 1980, vol. 76, p. 276.
40. Nicholas, J.E., Amodio, C.A., and Baker, M.J., *J. Chem. Soc., Faraday Trans.*, 1979, vol. 75, p. 1868.
41. Hochanadel, C.J., Sworski, T.J., and Ogren, P.J., *J. Phys. Chem.*, 1980, vol. 84, p. 231.
42. Becker, K.H., Engelhardt, B., and Wiesen, P., *Chem. Phys. Lett.*, 1989, vol. 154, p. 342.
43. Yee Quee, M.J. and Thynne, J.C.J., *Ber. Bunsen-Ges. Phys. Chem.*, 1968, vol. 72, p. 211.
44. Faubel, C. and Wagner, H.Gg., *Ber. Bunsen-Ges. Phys. Chem.*, 1977, vol. 81, p. 684.
45. Stachnik, R.A. and Molina, M.J., *J. Phys. Chem.*, 1987, vol. 91, p. 4603.
46. Braun, W., McNesby, J.R., and Bass, A.M., *J. Chem. Phys.*, 1967, vol. 46, p. 2071.
47. Fulle, D. and Hippler, H., *J. Chem. Phys.*, 1997, vol. 106, p. 8691.
48. Taatjes, C.A., *J. Chem. Phys.*, 1997, vol. 106, p. 1786.
49. David, D.C. and Moore, C.B., *J. Phys. Chem.*, 1995, vol. 99, p. 13467.
50. Devriendt, K., van Poppel, M., Boullart, W., and Peeters, J., *J. Phys. Chem.*, 1995, vol. 99, p. 16953.